Ultrasonic Assisted Assembly of Lignin Nanoparticles for UV-absorbent Thin Films

Dylan Damen Edmundson

A thesis

submitted in partial fulfillment of the

requirements for the degree of

Master of Science

University of Washington

2021

Committee:

Anthony Dichiara, chair

Rick Gustafson

Renata Bura

Eleftheria Roumeli

Program Authorized to Offer Degree:

School of Environmental and Forest Sciences

University of Washington

Abstract

Ultrasonic Assisted Assembly of Lignin Nanoparticles for UV-absorbent Thin Films

Dylan Damen Edmundson

Chair of the Supervisory Committee:

Assistant Professor Anthony Dichiara

The Department of Bioresource Science and Engineering

Lignin is a biproduct made from pulping wood and is the second most available biopolymer in the world. Although it is composed of useful aromatic and phenolic groups, making it a great UV absorber and antioxidant, its macrostructure is extremely complex and difficult to characterize and utilize with today's technology. In addition to these challenges, its characteristics can change based on the species of wood and type of pulping process used to extract the lignin. In the past lignin has been considered a waste rather than a high value product and is typically burned for energy, rather than utilizing its advantageous properties. Many recent studies have successfully found ways to valorize lignin by synthesizing nanoparticles from them for many applications such as: nanocomposite fillers for mechanical reinforcement, UV absorbing sunscreens and films, drug delivery, antioxidants, and many other applications.

Here lignin nanoparticles are synthesized from alkali lignin and used for UV absorption and mechanical reinforcement in a polyvinyl alcohol (PVA) polymer matrix. In chapter 1 ultrasonic forces were utilized for the self-assembly of bimodally distributed sizes of lignin molecules to a monodisperse particle solution. The pH dependence of the reactions was studied and a starting pH of 10.7 was found to create the best monodisperse nanoparticle solution with great colloidal stability, having a particle diameter of 204 nm and a zeta potential of -60 mV. In chapter 2 these particles were investigated for their UV and mechanical reinforcement. With only a 2.5 wt% addition of lignin nanoparticles the SPF value of the films increased from 0 to 26. At the same nanoparticle loading the ultimate tensile strength of the PVA nanocomposite was increased from 41 MPa to 60 MPa, the elastic modulus increased from 1256 MPa to 1713 MPa, while the change in strain in break was not statistically significant. In chapter 3 an acetylation reaction was done on the lignin and resulted in superior UV performance with an increase to 33 SPF, however the mechanical reinforcement suffered greatly. The research done here has shown that with science, technology, and innovation that lignin can be converted into a high value product.

Contents

List of Figures

List of Tables

Introduction

UV radiation is light that emits in the range of 200 to 400 nm consisting of UVA (400 – 320 nm), UVB (320 – 290 nm), and UVC (290 – 200 nm) [1]. Although the ozone layer absorbs essentially all UVC light, most UVA and UVB light transmit through and pose a severe risk to human health. It has been shown that radiation in the range of 290 – 500 nm can cause damage to DNA leading to cancer[2]. Additionally, UV light can increase the rate of degradation of organic materials leading to the breakdown of polymers and pharmaceutical medicines [3]. To protect against UV radiation metal oxides have been studied as UV absorbers and several publications have been successful incorporating particles made from ZnO [4] and TiO_2 into polymers [5]. Although successful, ZnO possess environmental and health concerns [6], [7] and TiO_2 increases photocatalytic activity, speeding up polymer degradation, making it ill-suited for applications in composite materials [8]. Furthermore metal oxides have wide band gaps resulting in a narrow UV absorption band [9].

Lignin is a vastly abundant biopolymer, second only to cellulose, consisting of highly conjugated aromatic structures with many phenolic hydroxyl and aryl ether linkages [10], [11]. The conjugated structures make lignin a great UV absorber with a broad absorption band allowing it to absorb harmful UV radiation [1], [11]–[14]. Additionally it operates as a free radical scavenger making it a great antioxidant [15]–[17]. Lignin is also used as a nanocomposite filler for reinforcement of waterborne polymers. The Phenolic hydroxyl groups can create hydrogen bonds with waterborne polymers enhancing mechanical properties [13], [15], [18]. When incorporated into a polymer matrix of poly(vinyl) alcohol (PVA) the composite can serve

many industrial applications such as: packaging, industrial paper and textile sizing, medical implant devices, drug delivery, and active packaging [10], [15], [19], [20].

Although lignin has many great features, its macroscale limits its ability to reinforce, and only small concentrations can be added to a polymer matrix before strengthening properties are hindered. It is possible to convert lignin into nanoparticles improving these properties [16], [21], [22]. Smaller sized particles increase the surface area available for bonding increasing the strength of the composite, however particles that are too small or have a bimodal distribution can lead to a drastic increase in elastic modulus and create an extremely brittle material [12], [21], [22]. Some studies have also found improved performance in UV absorption with reduction from the micro to nano scale [14]. It is also possible to enhance UV performance through acetylation reactions by increasing the degree of conjugation [23].

Previous studies have used ultrasonic irradiation for both top-down synthesis of nanoparticles and bottom up synthesis of macro particles formed from a lignin precursor [10], [24]. Ultrasonic forces cause cavitation leading to the formation and immediate collapse of air cavities, releasing energy [25]. This energy release can cause the homolytic cleavage of aryl ether bonds as well as generation of hydroxy and superoxy free radicals and, through reaction propagation, lead to depolymerizing or polymerizing reactions causing either an increase or reduction in particle size [24]. In this study ultrasonic forces grouped with pH control were investigated to convert bimodally distributed nanoparticles into a uniform monomodal distribution via ultrasound assisted assembly. The synthesized particles were then investigated for their UV absorption and mechanical reinforcement in a PVA matrix for thin film applications.

Chapter 1: Ultrasonic Assisted Self-Assembly of Lignin Nano Particles (LNPs)

1.1 Materials and Methods

1.1.1 LNP Synthesis

The lignin used in this study was Alkali lignin purchased from Tokyo Chemical Industries as a dry powder. For pH Adjustment 1 N HCl and 1 N NaOH were purchased form Fisher Scientific. The Alkali lignin was first redispersed in DI water to make 60 ml of a 0.5 wt% solution. Next the solution was pH adjusted to either 3.7 or 10.6 using HCl and NaOH. The solution was stirred for 30 min and then allowed to soak overnight. 30 ml of both acidic and basic samples were set aside and were referred to as samples A0 and B0.

Sonication was done using a 750 W, 20 kHz, 15-amp sonic horn, Sonic and Materials inc. VCX750. The horn was equipped with a micro cavitation probe with a 13 mm diameter and 114 μm amplitude. 10 ml of solution was separated out from the 3.7 and 10.6 pH solutions and placed into vials. The vials were placed into an ice bath and the solution was horn sonicated for 3 hours at 40% maximum amplitude, replacing ice as it melted. The solution was left to settle overnight to allow larger particles to sediment out of the solution and the solution containing the lignin nanoparticles (LNPs) was decanted off the top. Three replicates were made for both the acidic and basic pH's and were combined for film synthesis and particle characterization. These samples will be referred to as samples A3 and B3.

1.1.2 LNP Characterization

Transmission Electron Microscopy (TEM)

A Droplet of the full concentration LNP solution was drop cast onto a 200-mesh carbon coated grid and then stained by UranyLess Stain for 2 minutes. The sample measurements were taken on a FEI Tecnai F20 TEM operating at 200 kV. Particle diameter measurements were made using imageJ software. TEM images were used to study the morphology and size of the nanoparticles.

Hydrodynamic Diameter and Zeta Potential

Hydrodynamic diameter was determined by dynamic light scattering (DLS) using an Anton Paar Litesizer^{TM} 500 with a 40 mW laser with a fixed wavelength of 658 nm. To minimize multiple scattering effects samples were diluted to 0.5 mg/ml and measurements were taken using a backscattering angle of 175^{o}. Sample data was averaged over 3 repetitions, each consisting of 6 – 15 runs. DLS was used to study the size of the particles with different treatments.

Zeta potential was determined by electrophoretic light scattering (ELS) using the same equipment used for DLS. The samples were diluted to 0.5 mg/ml and the voltage was set to automatically adjust with a maximum voltage of 200V. Electrophoretic mobility was converted to zeta potential using the Smoluchowski approximation which is best suited for aqueous solution. Sample data was averaged over 3 repetitions, each consisting of 100 – 1000 processed runs. All data for DLS and ELS was processed using Anton Paar's built in processing software. Zeta potential was used to study the colloidal stability of the LNPs and their surface charge.

Fourier Transform Infrared Spectroscopy (FTIR) of Lignin Powders

FTIR measurements were taken using a Shimazu co. IR Prestige 21 FTIR. Lignin solutions were dried in an oven and then ground to a powder. The samples were then allowed to acclimate in a humidity-controlled room to ensure uniform moisture content between samples, and then one measurement was taken per sample. Measurements were taken from 550 – 4000 cm^{-1} using the Happ-Genzel anodization with a resolution of 4.0 cm^{-1} and 40 scans per measurement. Due to the high number of aromatic groups in lignin the band at 1600 cm^{-1}, which can be associated with lignin's aromatic skeletal vibrations [26], was used as a reference to normalize data for comparison. Since all lignin samples are expected to retain their aromatic character, these intensities should represent a baseline absorption for lignin samples which can be used for normalization. The sample data was normalized according to the equation A_x/A_{1600} where A_x is the absorption at wavelength x and A_{1600} is the absorption at 1600 cm^{-1}. The data was then translated to match baseline adsorption in the 4000 – 4500 cm^{-1} range of the basic samples and the acidic samples for comparison. FTIR of the powders was done to study the functional groups and structural changes of the LNPs.

1.2 Results and Discussion

1.2.1 Effects on Particle Size and Distribution

Particle size and size distribution uniformity has a large influence on material properties. With uniform particle sizes the void fraction of a polymer matrix is able to be filled with reinforcing particles that can uniformly distribute loading forces applied to the matrix [27]. A non-uniform distribution will lead to weak points due to disruptions in the matrix from larger particles with low surface area per unit mass or smaller particles not large enough to properly reenforce the polymer matrix, leading to weak interfacial OH-bonding. For this reason, it is

important to be able to control particle size and have a uniform distribution without large variation. Figure 1.2.1 shows DLS data collected for both acidic and basic samples before and after 3 hours of sonication. By adjusting the LNPs to a pH of 10.6, sample B0 was able to individualize its particles yielding the smallest particle diameters with 3 peaks at approximately 1 nm, 8 nm, and 260 nm. This is likely due to deprotonation of the phenolic hydroxyl groups of the lignin, creating a higher electronegativity on the particle surface and improving electrostatic repulsion between particles and solution stability [28]. This can be confirmed by ELS measurements shown in figure 1.2.1 as an inset with zeta potentials of -48 mV for B0 and -34 mV for A0. With pH 3.7 particle aggregates are beginning to form, however dispersion stability

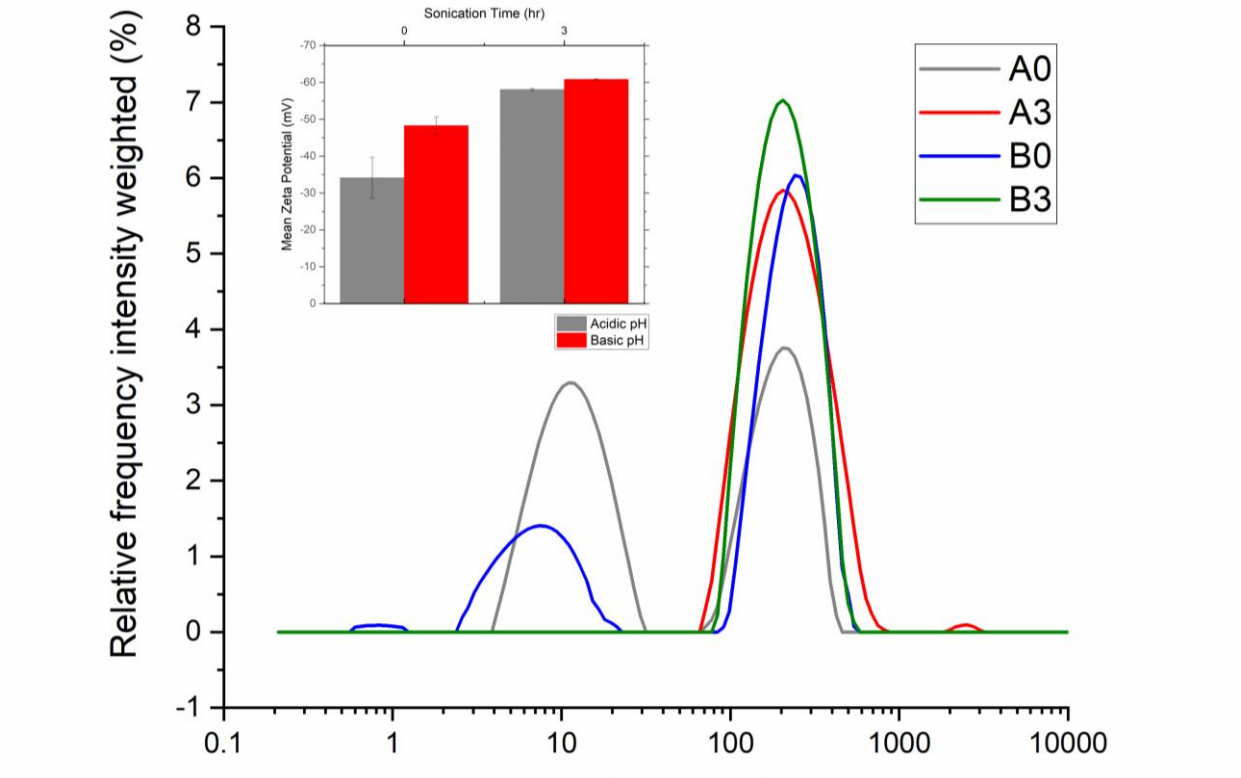

Figure 1.2.1 Particle diameter distribution taken from dynamic light scattering data for samples A0, A3, B0 and B3 with the zeta potential of acidic vs basic samples at 0- and 3-hours sonication inset.

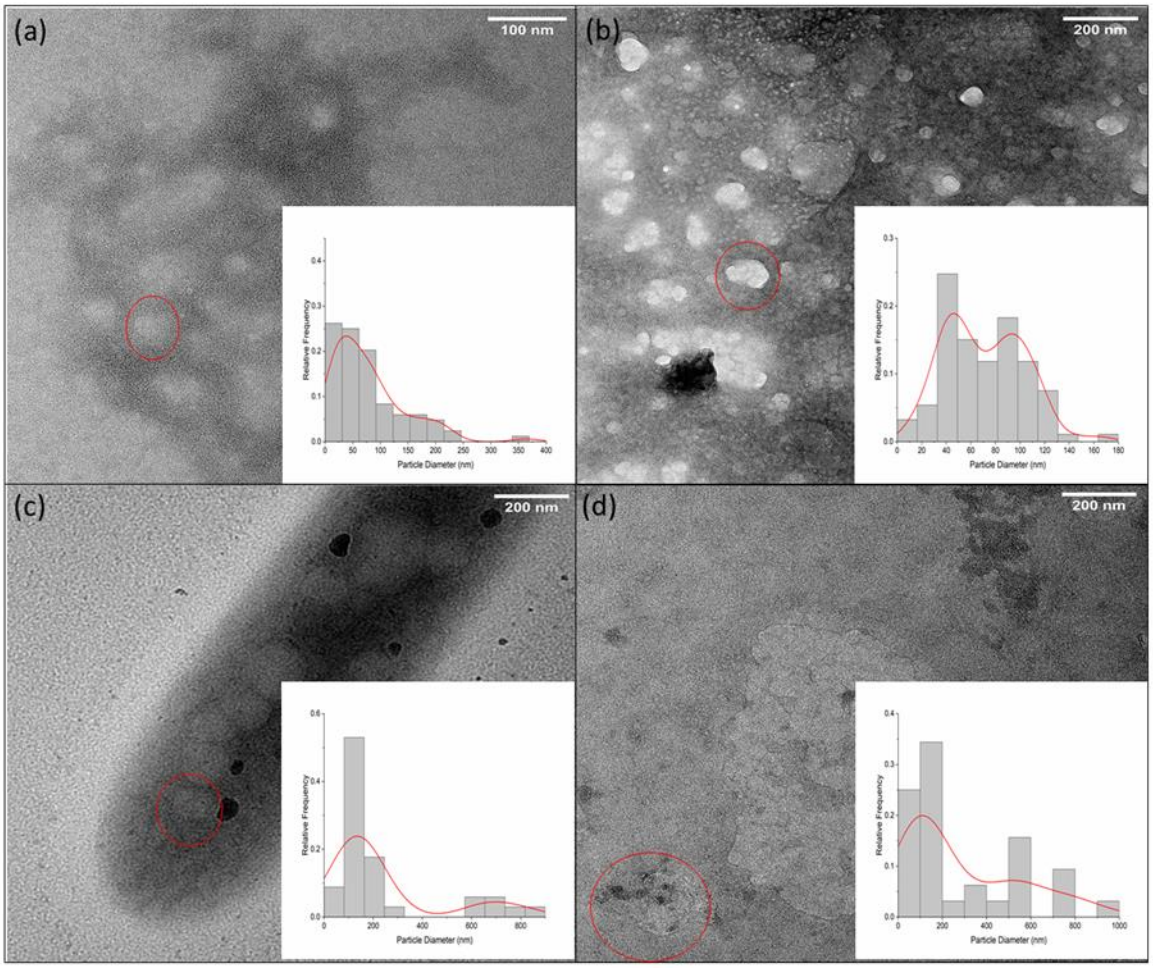

Figure 1.2.2 TEM imaging of samples A0 (a) A3 (b) B0 (c) and B3 (d) with corresponding size distribution generated using ImageJ software for measuring particle diameter.

is still good, and a bimodal distribution is achieved with peaks at approximately 11 nm and 200 nm. These results can be confirmed with TEM images in figure 1.2.2a (A0) and figure 1.2.2c (B0). The particles in (a) have more aggregates while (c) clearly shows individual particles.

After 3 hours of sonication DLS measurements show that both acidic and basic samples have monomodal peaks both at 204 nm. Although they have the same peak, sample A3 has a much broader distribution with a secondary peak occurring a 2520 nm, indicating poor separation of larger particles from the product solution during the sedimentation. Additionally, sample A3 has a broader peak ranging from 70 to 800 nm while B3 has sizes ranging from 80 to 600 nm. After sonication sample A3 had a pH of about 8 and B3 a pH of 9. Although pH changes occurred,

zeta potential for both samples decreased to -58 mV for A3 and -60 mV for B3 indicating great stability in solution. Iulian et al. proposed a mechanism consisting of simultaneous side chain cleavage (primarily β-O-4 bonds) and oxidative coupling leading to both polymerization and depolymerization between complex lignin chains [24]. In this study it is likely that oxidative coupling is the dominate termination pathway leading to polymerization and an increase in 4-O-5 and 5-5 condensed phenolic OH groups. This can be seen by TEM imaging shown in figure 1.2.2b and figure 1.2.2e, showing samples A3 and B3. These images no longer have individual spherical particles, but instead quasi spherical condensed groups of particles. Size distribution data taken from TEM images corroborate DLS measurements.

1.2.2 Chemical Composition and Hypothesized Reaction Pathway

FTIR was done on the dried lignin powders showing many complex absorption bands, shown in figure 1.2.3. The peak at 1030 cm^{-1} can be associated with β-O-4 lignin bonds [29]. For both acidic and basic samples, a decrease in intensity at this wavelength for sonicated samples was observed, indicating cleavage of β-O-4 lignin bonds. Additionally, the peak at 1125 cm^{-1} can be associated with aryl ether bonds and its shoulder at 1149 cm^{-1} may be caused by condensed structures [29]. The peak at 1125 cm^{-1} broadened while its shoulder was still present and appeared unchanged. These changes can be explained by the homolytic cleaving reactions proposed by Iulian et al. followed by lignin condensation reactions, primarily leading to 4-O-5 and 5-5 lignin bonds [24], [30]. Peaks between 1622 –1330 cm^{-1} were assigned to aromatic skeletal vibrations [31]. Peak broadening and shifting were observed with sonication for a peak occurring at 1591 cm^{-1} for samples A0 and B0 indicating more intermolecular interactions between aromatic units, which can be explained by molecules being more closely packed

matching the larger particle and monomodal dispersions seen in DLS results. The peak seen at 1268 cm^{-1} was likely caused by C=O and C-O stretching of guaiacyl groups [21]. Although a decrease in intensity was observed the intensity relative to nearby peaks appears unchanged between the sonicated and original sample, which may indicate little to no change to the guiacyl groups. Phenolic OH groups combined with aliphatic CH peaks occurred between 1480 – 1300 cm^{-1} [21]. These peaks appeared unchanged for basic samples, however significant peak broadening was observed for acidic groups, which may have been caused by a decrease in OH groups. Sonication processes may have also lead to the generation of superoxy and hydroxy free radicals which can react with lignin [24], [32]. With acidic conditions hydroxyl groups remain protonated leading to a positive dipole, potentially causing electrostatic attraction with superoxy

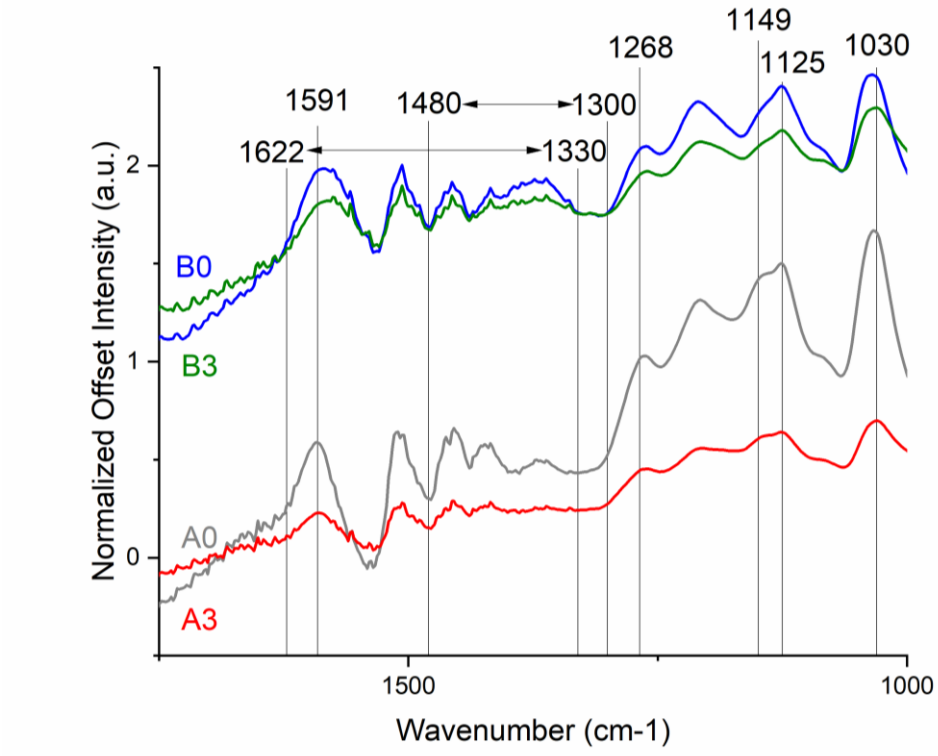

Figure 1.2.3 FTIR data collected from dried samples (powders) normalized by the absorption at 1600 cm^{-1}.

free radical anions. The superoxy radicals may then have reacted and deprotonated the OH groups like the mechanism shown in figure 1.2.4. On the other hand, with a basic pH, hydroxyl groups are deprotonated, and the negative charge repulses the superoxy anions inhibiting these reactions. The FTIR data shown in figure 1.2.4 shows the range (3500 – 3200 cm^{-1}) associated with OH groups [24], [26], [29]. For basic groups there is little to no change, however acidic groups see a large decrease in intensity. It is also notable that the basic samples do not have much of a peak in this region, however this is likely due to deprotonation of OH groups which may then form salts with Na cations while the lignin was dried to form a powder for testing. Tensile data (shown in the next section) reinforces these observations since acidic sonicated

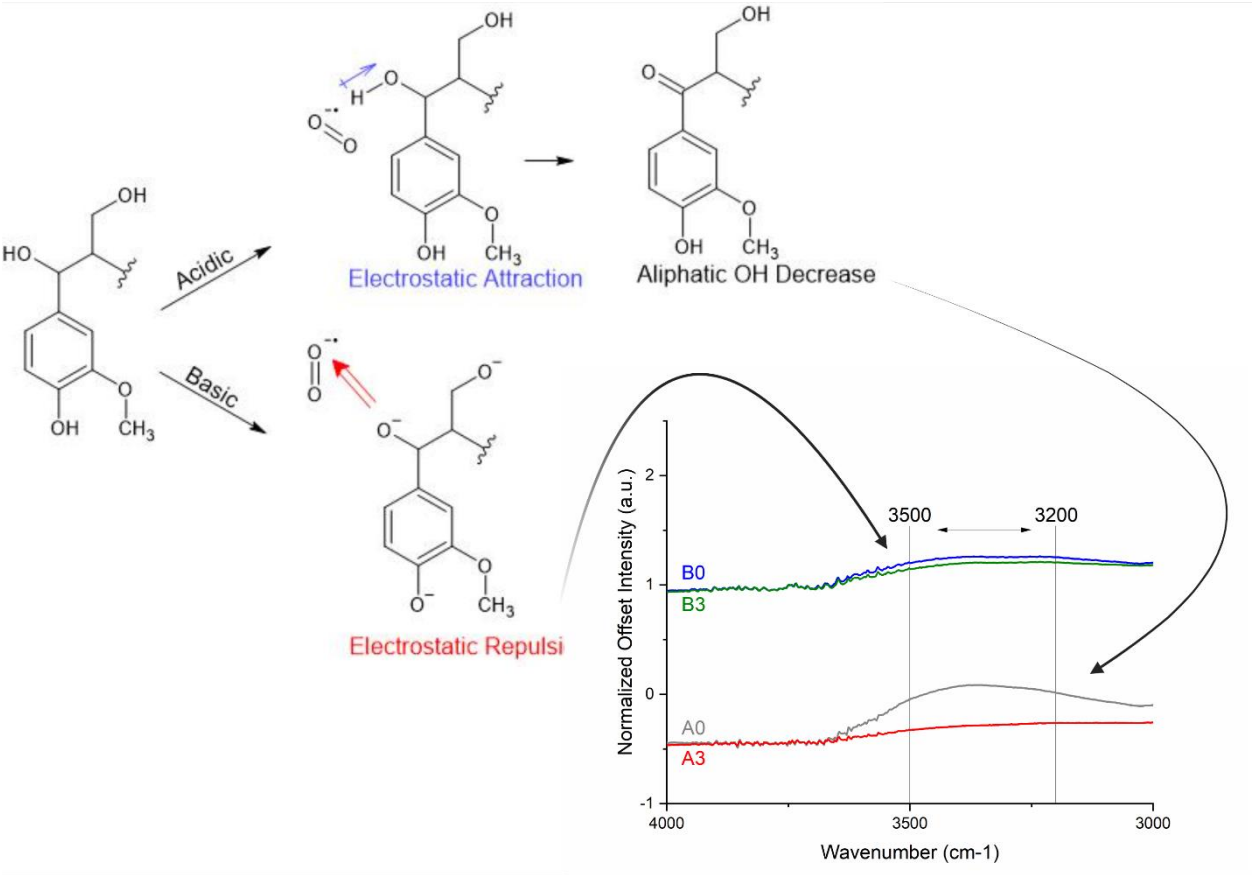

Figure 1.2.4 Depiction of possible reaction pathway explaining reason for decrease in OH functional groups for acidic sample.

samples were poor reinforcers for PVA while basic sonicated samples offered competitive mechanical reinforcement.

Chapter 2: LNPs in Polyvinyl Alcohol for Mechanical Reinforcement and UV-absorption

2.1 Materials and Methods

2.1.1 Nanocomposite Synthesis

The PVA used for film synthesis was purchased from sigma Aldrich and had a molecular weight of 89,000 – 98,000 g/mol and was 99+% hydrolyzed. 500 mg nanocomposite films were prepared by first dissolving PVA in DI water at 90 ^{o}C stirring at 600 RPM for 30 minutes to form a 5 wt% solution. The PVA solution was removed from the heat and allowed to cool to room temperature before adding the lignin solution to the mixture to form the appropriate solution concentration. DI water was added to the mixture and the solution was topped off to make a 2 wt% solution. The solution was degassed in a sonic bath for 1 minute, poured into a Pyrex Glass petri dish, and allowed to dry in an oven at 60 ^{o}C overnight. Films were removed from the petri dish and allowed to acclimate in a humidity-controlled room for 24 hours before testing (50% +/- 2% relative humidity and 23 ^{o}C +/- 1 ^{o}C). The final prepared films consisted of 3 replicates for 0, 2.5, and 5 wt% LNP loadings based on solids for each sample of LNP made.

2.1.2 Characterization

FTIR of Films

FTIR measurement were taken on the same equipment with the same settings as FTIR done on LNP powders in chapter 1. Five measurements were taken, one at the center, and 4 rotating a quarter turn clockwise around the circular film. Each measurement was normalized and then the

5 normalized measurements were averaged. Normalization was done according to the equation A_x/A_{839}, where A_x is the absorption at wavelength x and A_{839} is the absorption at 839 cm^{-1}. Wavenumber 839 cm^{-1} was chosen for normalization since it is associated with PVA's conformation [15] which was not observed or expected to change. Finally, the data was translated vertically so the baseline absorption values were equivalent. FTIR of the films was done to study the molecular interactions between the LNPs and PVA matrix.

Scanning Electron Microscopy (SEM)

SEM images were taken using a TFS Apreo-S with Lovac SEM. The samples were dipped in liquid nitrogen for 5 min, and then placed on a glass slide. A razor blade was gently placed where the fracture was desired, and a hammer was used to lightly tap the razor and fracture the sample. The sample was then placed in a dehumidifier, coated with 4 nm of Pt using vapor deposition, and then mounted on carbon tape. Measurements were taken using an accelerating voltage of 2.0 kV and the cross section of the sample was observed. SEM was used to study the morphology of the film and the particle dispersion inside the matrix.

Smoothness

Smoothness measurements were done using a Hagerty Technologies Model 538 Paper Smoothness tester and tested according to the Technical Association of the Pulp and Paper Industry (TAPPI) standard T479 cm-09. The tester measured the time for a volume of air to seep between the sample and a smooth glass plate, the rougher the surface the faster the air leak. Five measurements were taken, one at the center, and 4 rotating a quarter turn clockwise around the circular film and the 5 measurements were averaged for each sample. Smoothness measurements were taken in conjunction with SEM to study the effects of LNP particle size on the surface morphology of the films.

UV-vis Spectroscopy

UV-vis measurements were taken using a Perkin Elmer UV-vis Lambda 750 Spectrometer with 100 mm InGaAs integrating sphere using an InGaAs wafer as the 100% transmission background to assess the UV absorption capabilities of the LNP/PVA nanocomposite films. Measurements were taken from 290 – 800 nm in 5 nm increments at 5 locations around the film and averaged in the same fashion as was done for smoothness and FTIR. To assess the stability of the LNP/PVA composites the films were exposed to artificial UV light generated from a Reptisun 10.0 UVB 13 W light bulb for 3 days and then remeasured. SPF values were calculated according to the Mansur equation [33].

$$SPF = 10\ x \sum_{290}^{320} EE(\lambda)\ x\ I(\lambda)\ x\ Abs(\lambda)$$

Where Abs(λ) is the absorption and EE(λ) x I(λ) is the erythemal effect spectrum times the solar intensity spectrum at wavelength λ, shown as tabulated data in 5 nm increments by L. Mbanga et al [33]. For comparison with other publications increase in absorption and decrease in transmission were calculated using.

$$X_{350}\ or\ X_{550} = \frac{\%T_0 - \%T_L}{\%T_0}\ x\ 100\%$$

Where X_{350} is the increase in absorption at 350 nm, X_{550} is the decrease in transmission at 550 nm, $\%T_0$ is precent transmission for pure polyvinyl alcohol and $\%T_L$ is for the percent transmission for films loaded with varying LNP loadings.

Thermogravimetric Analysis (TGA)

TGA measurements were taken using a TA Instruments TGA Q50 to assess the thermal stability of the nanocomposite films. Samples were heated in a platinum pan under a nitrogen gas

flow rate of 40 ml/min. The heating rate was 10 ^{o}C/min and the temperature ranged from 30 ^{o}C to 600 ^{o}C. The first derivative of the data was calculated numerically and plotted over the TGA data. TGA was used to assess the thermal stability of the nanocomposite films.

X-Ray Diffraction

X-Ray Diffraction measurements were taken to assess the crystallinity of the films. Samples were mounted on a silicon dioxide wafer and a Bruker D8 powder diffractometer, equipped with a microfocus X-ray source producing X-rays with high-efficiency Cu (1.54056 Å) anode working at 50 kV and 1000 μA. The beams were focused using a 0.50 mm beam collimator and a Pilatus 100K large area 2D detector was used to record diffractograms. Scanning was done from 0^{o} to 90^{o} with 11^{o} increments and a 30s scan time per increment. Crystallinity was estimated by:

$$\frac{A_c}{A_{total}}$$

Where, A_c is the area under the crystalline region of the diffractogram and A_{total} is the area under the amorphous and crystalline regions.

Tensile Testing

Tensile testing was done using a Thwing Albert Model 1760 Tensile Tester according to ASTMD882-10 to assess the extent of mechanical reinforcement of PVA films by LNPs. The films were cut into 70 mm x 15mm strips. Each strips' thickness was measured in 3 places and averaged. Tabs were taped at the edge of the samples to help prevent damage from testing clamps and three replicates were performed for each sample. Wet tensile samples were measured in the same manner, except the center of the samples were dipped into a DI water bath for 2 seconds to disrupt hydrogen bonding and then tested. Raw data for all tensile measurements was

averaged using the equal arc segment method described by Zhong and Wille [34]. Increase in elastic modulus and ultimate tensile strength (UTS) were calculated to compare sample data to other publications using the following equations:

$$X_{UTS} = \frac{UTS_L - UTS_0}{UTS_0} \; x \; 100\%$$

$$X_E = \frac{E_L - E_0}{E_0} \; x \; 100\%$$

Where X_{UTS} is the increase in UTS, UTS_L is the UTS of LNP loaded films, UTS_0 is UTS of pure PVA, X_E is the increase in elastic modulus, E_L is elastic modulus of LNP loaded films, and E_0 is elastic modulus of pure PVA. Wet strength retention was calculated using the following equation:

$$WS = \frac{UTS_{wet}}{UTS_{dry(ave)}} x100\%$$

Where WS is the wet strength retention, UTS_{wet} is the UTS of the wetted sample, and $UTS_{dry(ave)}$ is the average UTS of the dry sample.

Water Stability

Films were cut into 30 mm x 10 mm samples and their weights were recorded. The samples were then placed into scintillating vials with 20 ml of DI water. The vials were incubated for 1 day at 40 RPM and the samples were then removed and dried. The dry weights were recorded, and the weight loss was calculated using the following mass ratio:

$$X_M = \frac{M_f - M_0}{M_0} \; x \; 100\%$$

Where M_f is the final mass, M_0 is the initial mass and X_M is the weight loss ratio. Stability testing was done to assess the nanocomposites sensitivity to water.

2.2 Results and Discussion

2.2.1 UV-vis Film Performance

The nanocomposite film's ability to UV-absorb and transmit visible light was assessed from 290 – 800 nm. Figure 2.2.1 shows the transmission spectrum for all samples with a fixed concentration of 2.5 wt%, while the inset shows sample B3 at varying LNP concentrations before and after UV exposure. All nanocomposite samples absorbed essentially all UVB and most UVA light, while retaining good visible transmission. Sample B3 had the lowest transmission in the UV range while A0 had the highest transmission in the visible range. Since sample A0 has smaller particles, they are able to disperse more uniformly in the matrix, filling voids in the matrix and leading to better transmission [35]. B3 has the highest UV absorption, likely due to a higher degree of conjugation broadening the range of possible quantized π-π* transitions[11],

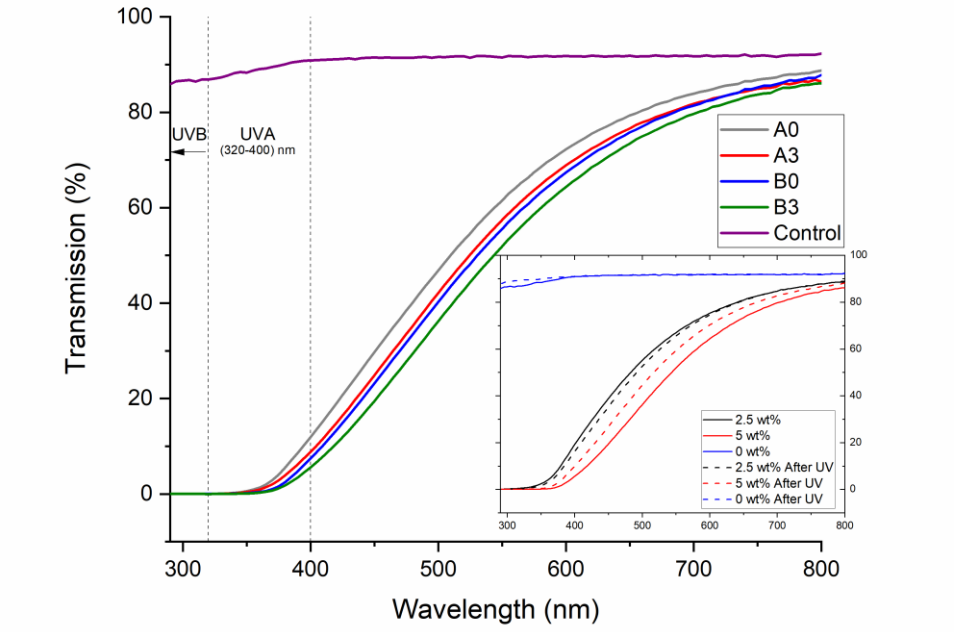

Figure 2.2.1 UV-vis transmission data for all composites compared to pure PVA with sample B3 transmission at different particle loadings before and after prolonged UV exposure inset.

[36]. The inset in figure 2.2.1 shows an absorption increase with increasing concentration, while transmission in the visible range decreases. The particles also show good stability with little to no change in UV absorption after being exposed to UV light for 3 days.

Figure 2.2.2 shows calculated SPF values, the mean visible light transmission, and the average transmission at 550 nm for pristine PVA, and sample B3 at 2.5 and 5 wt%. SPF values of sample B3 were found to improve significantly (t-test p-value of 0.01) from 25.8 to 35.9 with increasing LNP loading from 2.5 to 5 wt%. However, LNP loading at 2.5 wt% had the best

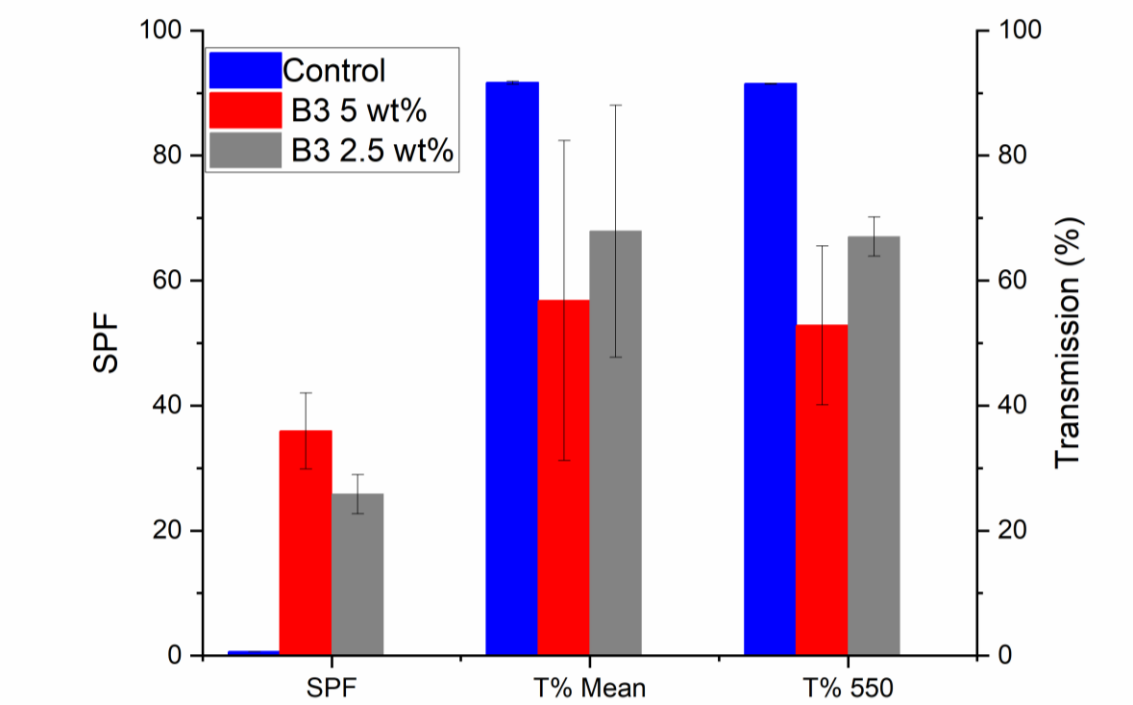

Figure 2.2.2 SPF, mean visible transmission, and transmission at 550 nm for pure PVA, and sample B3 at 2.5 wt% and 5 wt%.

transmission in the visible range making it a good UV absorber with great visibility through the film making B3 at 2.5 wt% the best candidate for UV absorbent transparent films. Figure 2.2.3 shows an Ashby plot comparing sample B3 at 2.5 and 5 wt% loading with other related publications [12], [13], [15], [17], [18], [22], [37], [38]. The ideal UV-vis characteristics for these

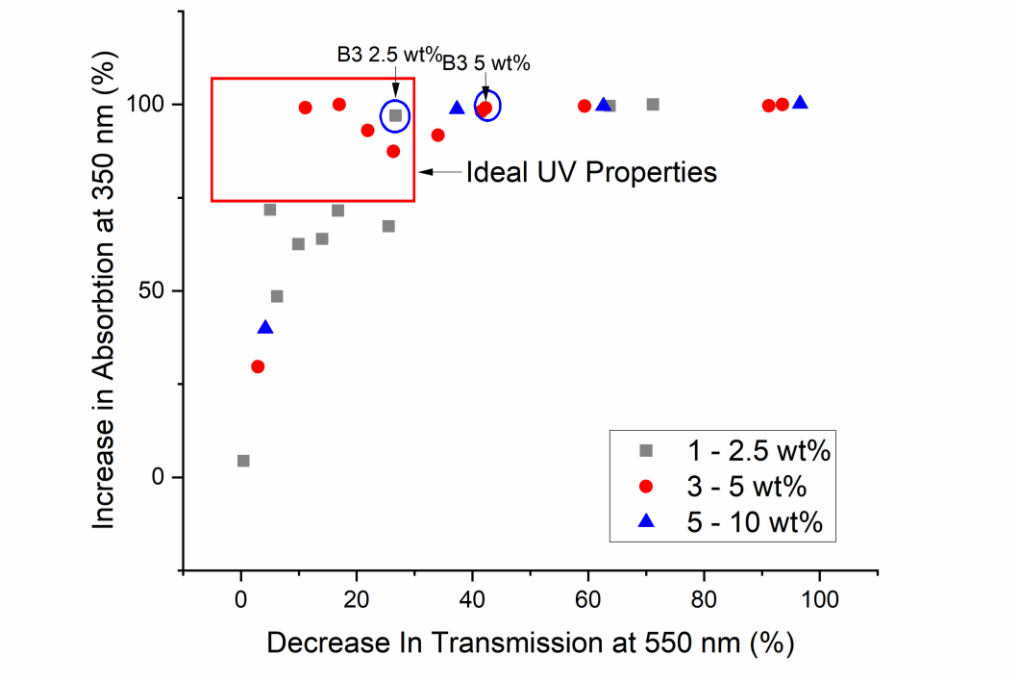

Figure 2.2.4 Ashby plot comparing data from references X_{350} and X_{550} for comparison.

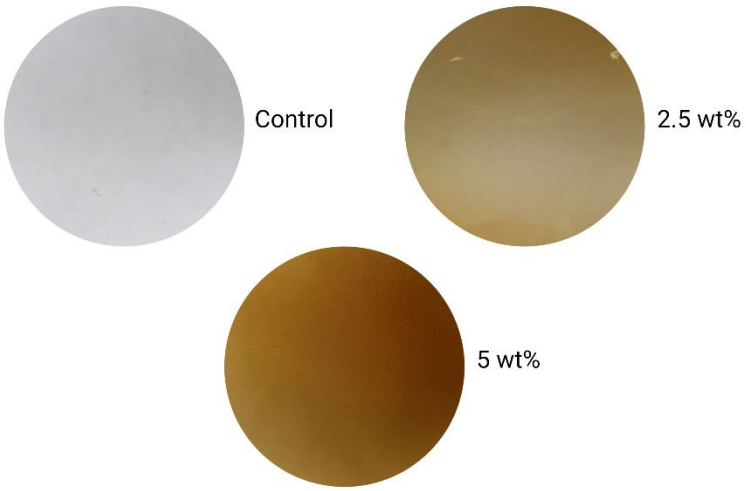

Figure 2.2.3 Image of Pure PVA (top left) sample B0 at 2.5 wt% (top right) and sample B0 at 5 wt% (bottom).

films would be a large increase in absorption at 350 nm without a decrease in transmission at 550 nm. Figure 2.2.3 shows that B3 2.5 is in the top 5 UV absorbent PVA/LNP nanocomposites currently published. Figure 2.2.4 shows an image of the pure PVA control and sample B0 at 2.5 and 5 wt%. At 2.5 wt% the sample is still very transparent and the particles appear to have good

formation and uniform distribution through the film, however with an increase to 5 wt% the film becomes very dark and the dispersion while still good begins to diminish with the right side appearing slightly darker.

2.2.2 Nanocomposite Mechanical Performance and Stability

Mechanical properties are important to be able to assess a materials' possible applications. Of these, tensile strength and elastic modulus are some of the most important aspects. Testing was done for all samples, however only sample B3 exhibited mechanical reinforcement. This was likely due to the nature of the particle formation mechanism discussed in the "Lignin Nanoparticle Synthesis" section. This leaves a larger amount of OH groups available for hydrogen bonding which is the primary mechanism that PVA nanocomposites are reenforced by [21]. Figure 2.2.5a shows UTS, elastic modulus, and elongation at break for sample B3 at varying LNP loading and figure 2.2.5b shows the averaged stress and strain data. From both figures it is evident that the UTS and elastic modulus increased with increasing LNP loading showing mechanical reinforcement. Although there was a large increase in strength from 2.5 to 5 wt% by 9 MPa it is notable that the results were not significant within a 95% confidence interval (t-test p-value of 0.05). B3 5 had a large standard deviation and a larger elastic modulus and thus had suffered significant embrittlement compared to B3 2.5. Additionally, the elongation at break was greatly reduced with increasing particle concentration along with the area under the curve (Toughness), however with a very large standard deviation the results were found to be insignificant with a p-value of 0.086. Additionally, the resilience of the composite increases with increasing particle concentration. For applications such as food packaging it is important that

plastic alternatives are strong but retain a plasticity comparable to current packaging materials [15], [39]. For this reason, B3 2.5 was the better candidate for many applications. Wet tensile

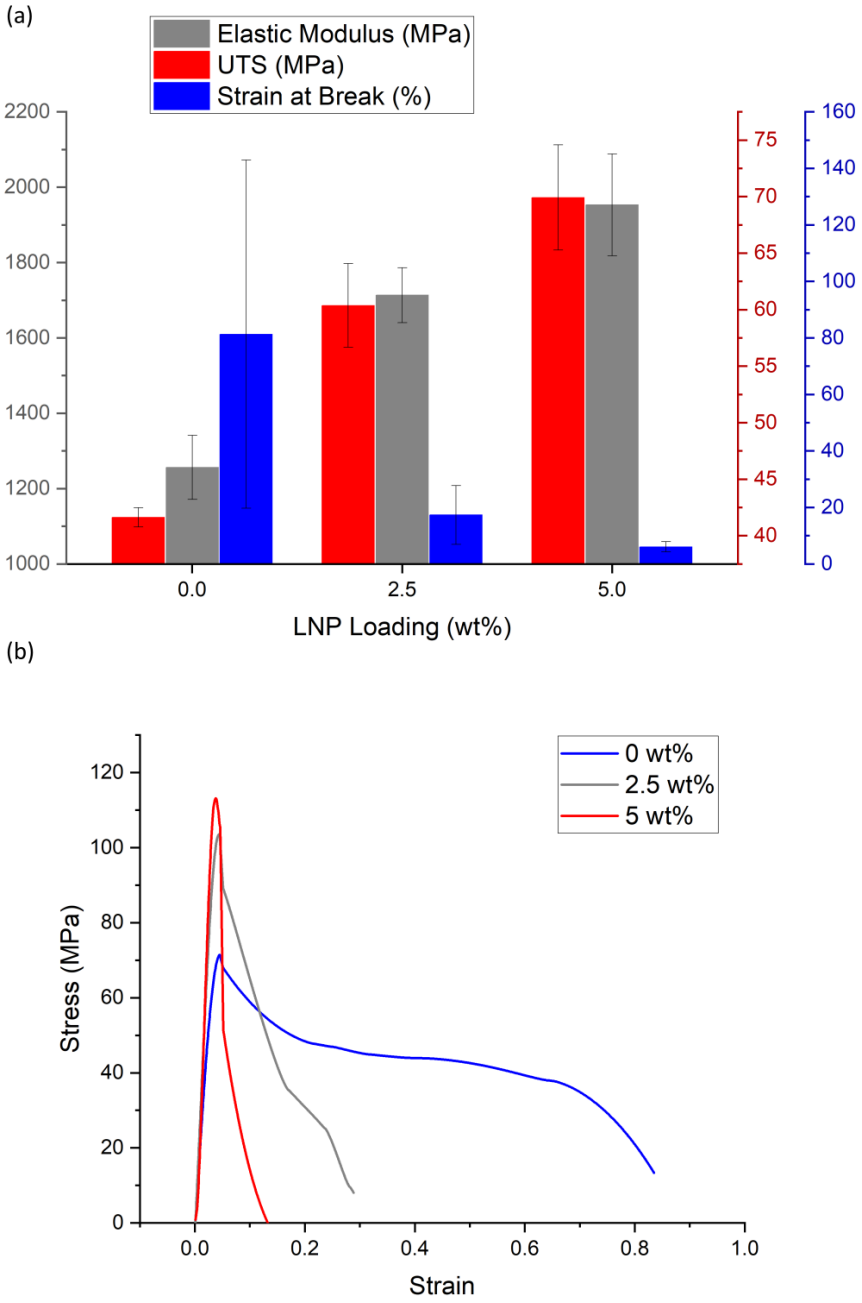

Figure 2.2.5 (a) Elastic modulus, ultimate tensile strength (UTS), and wet UTS of sample B3 at varying particle loading. (b) Stress strain curve of raw tensile data averaged using equal arc segment method.

testing was performed to interrupt hydrogen bonding to assess the properties of water-resistant

intermolecular bonding. Wet UTS was also improved for B3 2.5 compared to pristine PVA, with a slight increase in wet strength retention from 37% to 40%, however this was found to be insignificant with a t-test p-value of 0.69. Lignin is capable of hydrophobic interactions with other lignin molecules, which would increase wet strength retention, however since this was not

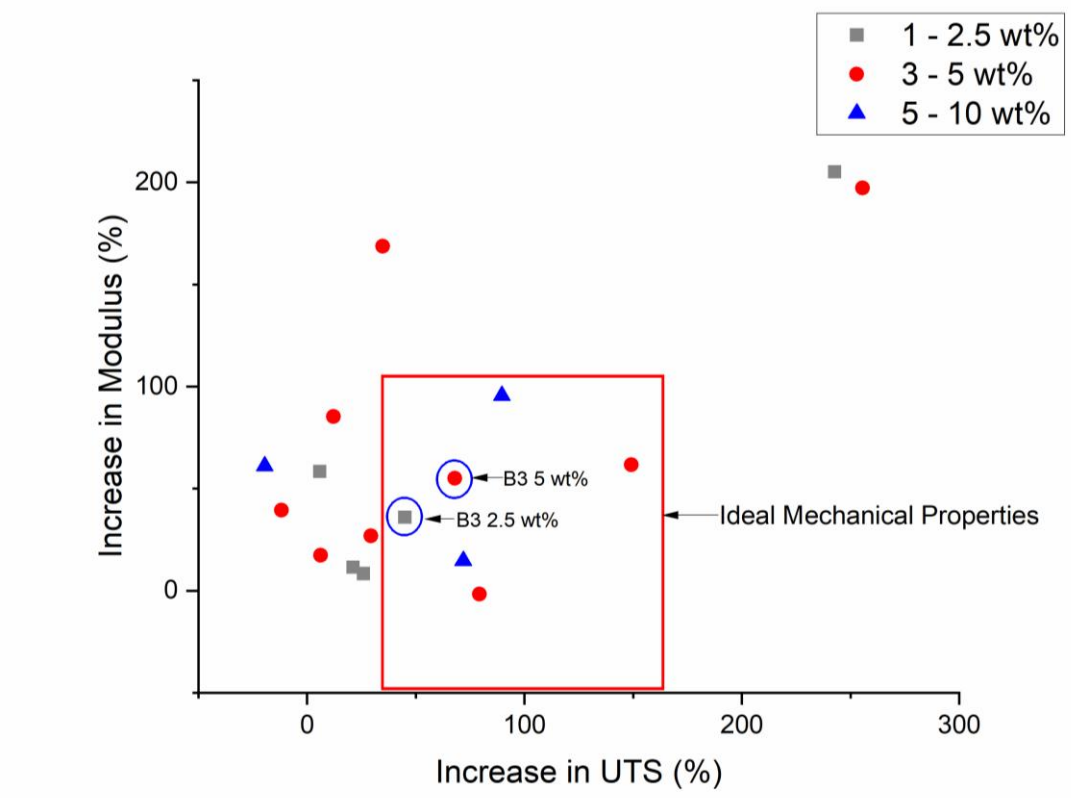

Figure 2.2.6 Ashby plot comparing increase in UTS with increase in modulus.

seen here it is likely that lignin molecules were not interacting, indicating that they were well dispersed throughout the PVA matrix.

Figure 2.2.6 shows an Ashby plot using increase in elastic modulus and UTS to compare the samples with other studies conducted with similar composites [12], [13], [15], [18], [21], [37], [38], [40]. To maximize the effectiveness of the films an increase in UTS and elastic modulus was desired, however if elastic modulus increased too much then the film would become too brittle [39]. The region with ideal characteristics is shown on the plot and sample B3 2.5 and B3

5 were both within the top 6 values. With sample B3 2.5 having comparable UTS and significantly lower elastic modulus it retained its plasticity well and is likely the best option for most thin film applications.

2.2.3 Nanocomposite Characterization

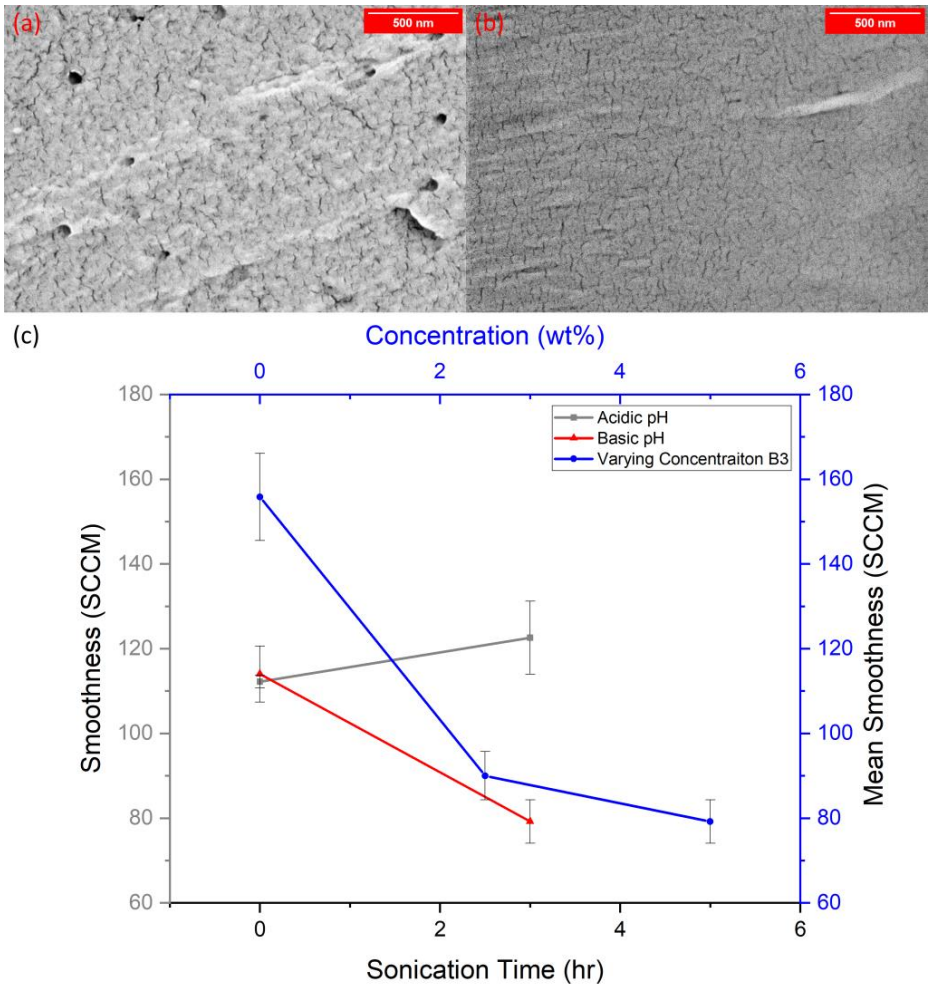

Figure 2.2.7 (a) Cross section SEM image of cryofractured samples B3 at 2.5 wt% and (b) Pure PVA. (c) Smoothness data taken for films at varying concentrations (red) and of samples containing 5 wt% LNP loading with varying sonication times for basic (blue) and acidic (black) pH.

To support several observations for the UV-vis and mechanical properties, other characterizations were done. Figure 2.2.7a shows SEM images of the cryofractured sample B3

2.5 and 2.2.7b shows SEM of pristine PVA. The SEM shows particles uniformly distributed throughout the thickness with few particle aggregates. Smoothness data shown in figure 2.2.7c also shows an increased smoothness with increasing particle concentration for sample B3. As voids in the PVA matrix were filled with LNPs the surface had less valleys leading to a uniform and smooth surface [41]. It can also be seen that with sonication, basic samples experienced better smoothness at a controlled LNP loading while acidic samples got worse. Poor interfacial bonding in the PVA matrix can cause lignin nanoparticles to aggregate and prevent them from

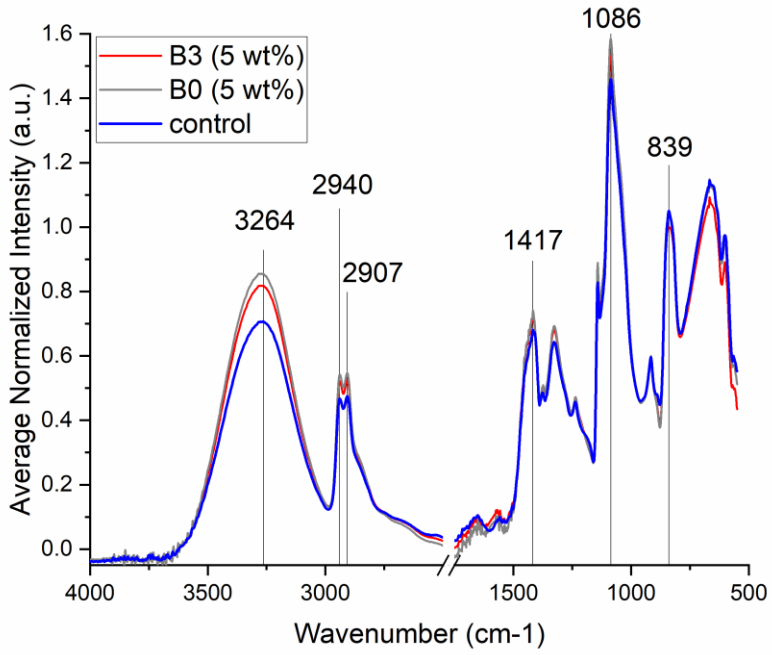

Figure 2.2.8 FTIR data collected for pure poly(vinyl) alcohol (control) and samples B0 and B3 at 5 wt%.

filling voids in the matrix.

FTIR was also performed on films to see how LNPs interacted with the PVA matrix. Figure 2.2.8 shows the FTIR spectra for pristine PVA and sample B0 and B3 at 2.5 wt% LNP loading. Peaks at 3264 cm^{-1} were assigned to O-H stretching vibrations, and peaks at 1086 cm^{-1} and 1417

cm^{-1} were related to C-O bonds of alcohols [42]. An increase in peak intensity from the control to B0 for these peaks showed an increase in OH groups, while peak broadening of B3 compared to B0 at 3264 cm^{-1} indicated an increase in OH intermolecular bonding. 2940 cm^{-1}, 2907 cm^{-1} and 839 cm^{-1} were indicators of PVA conformational changes [15]. No significant changes in

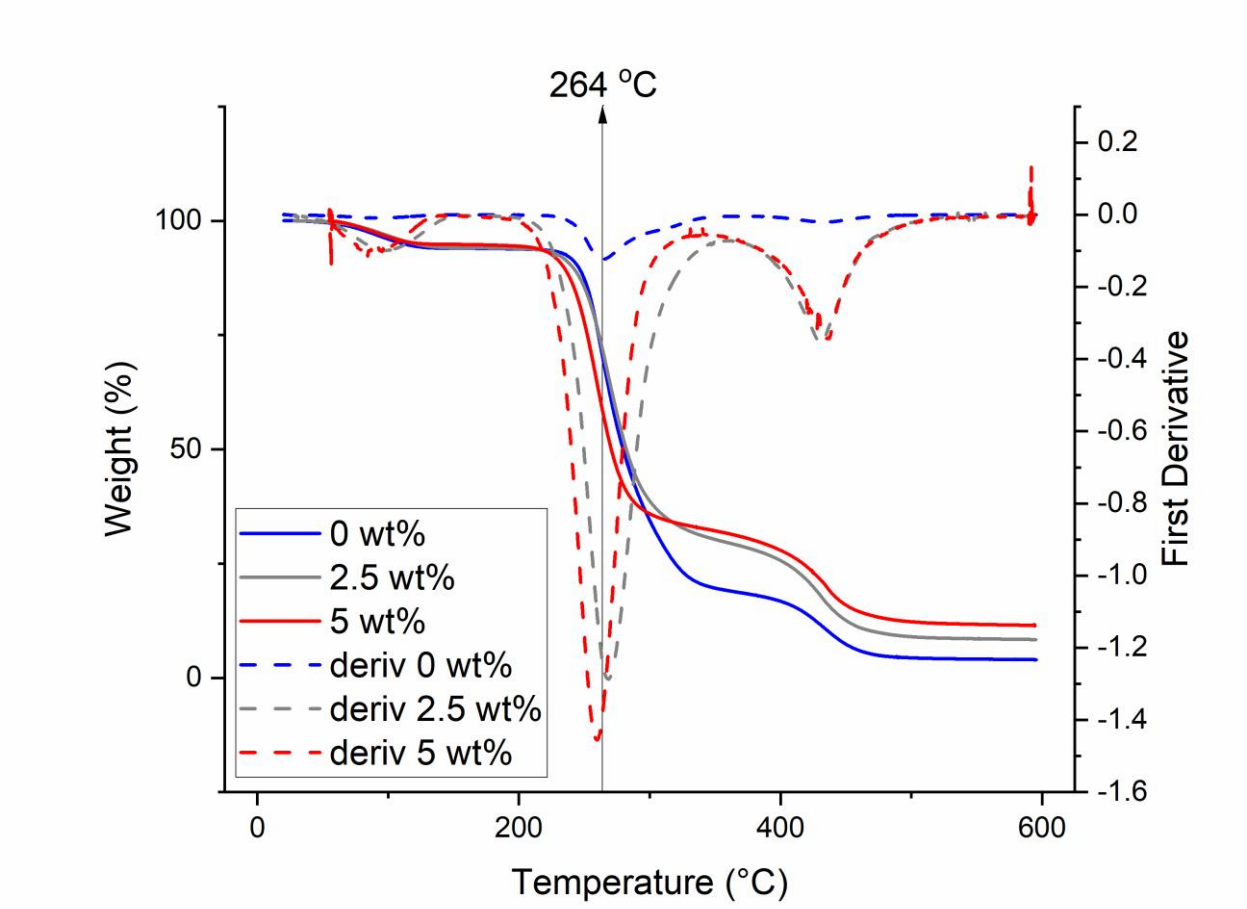

Figure 2.2.9 TGA data taken for sample B3 at varying concentrations and the corresponding first derivative.

peak shape were observed indicating no changes to PVA conformation.

Figure 2.2.9 and 2.2.10 show TGA (for sample B3 at 0 – 5 wt% LNP loading) and XRD data, respectively. Thermal stability is an important characteristic for plastics melt processing and the polymers degree of crystallinity can have great influence on its thermal stability. Figure 2.2.9

shows an Initial weight loss of approximately 6% for each sample from 30 – 120 ^{o}C which can be attributed to water loss. Then the initial PVA melting and decomposition from approximately 200 – 350 ^{o}C contributed another weight loss [43] starting at 94 wt% and ending at 20 wt% for PVA, 30 wt% for B3 2.5, and 32% for B3 5. Finale decomposition of the polymer, in which

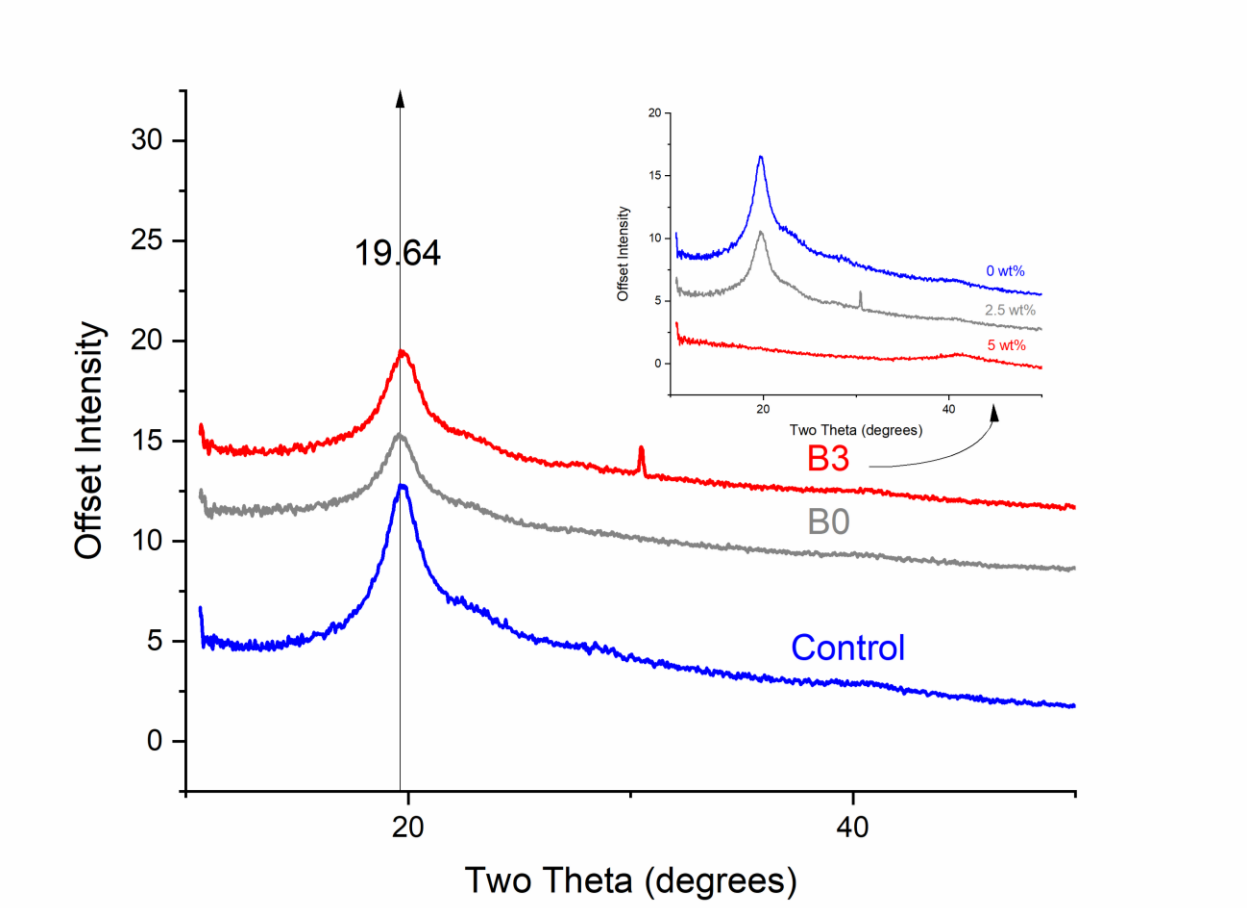

Figure 2.2.10 X-ray diffraction data for pure poly(vinyl) alcohol and samples B0 and B3 at 2.5 wt% with sample B3 shown with varying concentrations from 0 to 5 wt% as an inset.

PVA formed polyene structures and underwent chain cleavage from 375 – 480 ^{o}C [43], [44], occurred leading to a final weight of 4 wt% for PVA, 9 wt% for B3 2.5 and 11 wt% for B3 5. Figure 2.2.10's XRD data shows peak broadening and a reduction in intensity of the peak which occurred at 19.64^{0} which can be associated with the crystalline peak of PVA [45]. Crystallinity can be observed as the ratio of the area under the crystalline peak to the area under the entire

curve [46] and using this method it is possible to qualitatively and quantitatively compare crystallinities. Table 2.2.1 shows the estimated crystallinities for the control and samples B0 and B3 at 2.5 and 5 wt%. The table combined with figure 2.2.10 shows that sonication did not significantly change the crystallinity compared to sample B0, however increasing concentration of sample B3 greatly reduced the crystallinity of the sample.

With an addition of only 2.5 wt% LNP, a 10 wt% increase in residual mass was seen after the initial decomposition of PVA. This increase in thermal stability was likely due to lignin's ability to scavenge free radicals. As PVA chain scissions occurred, free radicals were generated and it is likely that lignin tied up these electrons hindering the degradation process [22]. It is notable that the decrease in crystallinity would be expected to cause the thermal stability to diminish by introducing more amorphous regions [47], however the effects of the free radical scavenging overwhelm this, further showing lignin's great quality as a thermal stabilizer. Additional lignin content led to 12 wt% increase in residual mass, further increasing the thermal stability. This same trend was seen for the range of 375 – 480 ^{o}C where, at 2.5 wt%, LNP loading caused a 5 wt% increase in residual mass and a 5 wt% LNP loading caused a 7 wt% increase.

Table 2.2.1 Calculated Crystallinity for all samples.

sample	2.5 wt%	5 wt%
Control	27.21%	27.21%
B0	19.80%	15.02%
B3	22.03%	0.00%

Stability testing was done with pristine PVA and sample B3 2.5 to compare its ability to biodegrade and solubilize in water. Addition of lignin showed no significant change in stability compared to pure PVA showing that the nanocomposite retains its ability to dissolve in water. This

is important for the nanocomposites' compatibility for many applications such as packaging, paper, and textiles [15], [20].

Chapter 3: UV Absorption Efficiency Maximization Via Acetylation of LNPs

3.1 Materials and Methods

3.1.1 Acetylated LNP Synthesis and Characterization

For comparison of UV absorption efficiency one sample of acetylated lignin was prepared and was referred to as sample AC. For the acetylated lignin reaction acetic anhydride 99+%, pyridine, and 200 proof ethanol were purchased from Fisher Scientific. The acetylation procedure was conducted similar to Kim et al. [23]. First 10 ml of acetic anhydride was mixed with 10 ml of pyridine. Next, 1g of alkali lignin was added to the solution and the mixture was bath sonicated for 3 minutes and then allowed to stir for 72 hours. The solution was then added dropwise to 500 ml of DI ice to precipitate out the lignin. The precipitate was filtered and washed with ethanol and cold DI water to remove residual pyridine and acetic anhydride. A duplicate sample was made and then horn sonicated; this sample was referred to as sample AC3. DLS, ELS, and FTIR were all conducted for the acetylated samples in the same manner as was done for samples in chapter 1.

3.1.2 Acetylated Lignin Film Synthesis and Characterization

The Acetylated samples were incorporated into PVA nanocomposites and then were characterized in the same manner as was done for films in chapter 2. However, only UV-vis and tensile measurements were taken of the films since these were the main characteristics in question.

3.2 Results and Discussion

3.2.1 Effects of Acetylation on Particle Size and Structure

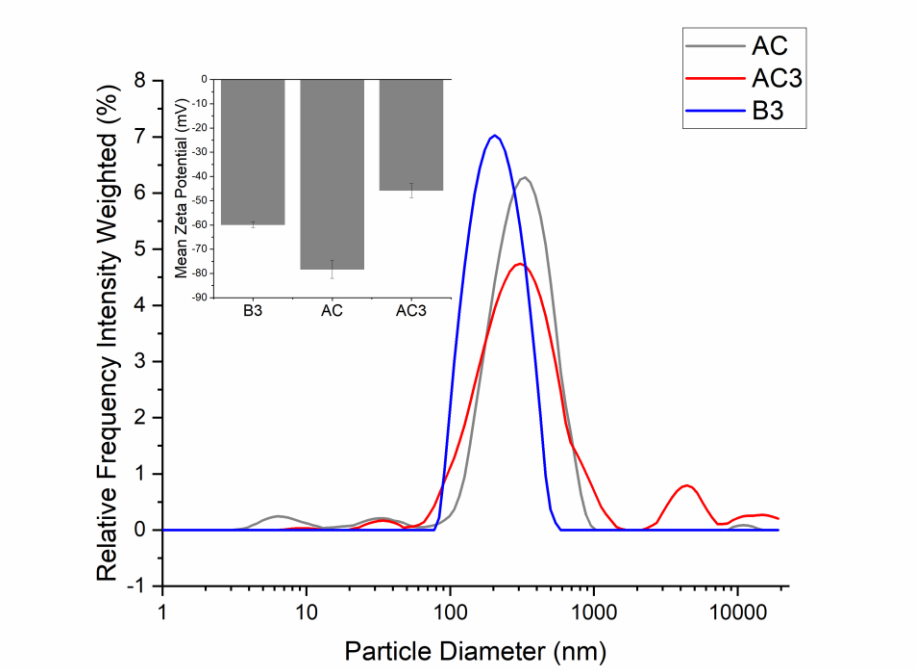

Figure 3.2.1 DLS and ELS measurements taken for sample acetylated lignin (AC), horn sonicated acetylated lignin (AC3) and sample B3 (best result from previous chapters).

Since sample B3 in chapters 1 and 2 led to the best results, this sample was used for comparison with the acetylated lignin samples. Figure 3.1.1 show the DLS results for samples B3, AC, and AC3 along with their ELS results inset. It can be seen from the figure that, with acetylation, the size distribution of the sample becomes very uniform with an average hydrodynamic diameter of 372 nm. This was likely due to the precipitation and filtration of the acetylated lignin. After the reaction was carried out much of the lignin was lost during the purification steps, likely causing smaller particles to be lost and leaving a uniform distribution. It can also be seen from the ELS measurements that the sample becomes even more electronegative with a zeta potential of -78 mV. This is likely due to C-OH groups being replaced by C-

$OCOCH_3$ groups, leading to more free electrons on the particle surface. With horn sonication the size distribution broadened, and much larger particles were developed from the self-assembly mechanism described in chapter 1. Additionally, the zeta potential decreased to -46 mV. This may have been caused by an increase in particle size, possibly caused by acetyl groups reacting during ultrasonication leading to lower surface area/g of particle and thus lower surface charge.

3.2.2 Effects of acetylation on UV-vis and Tensile Performance

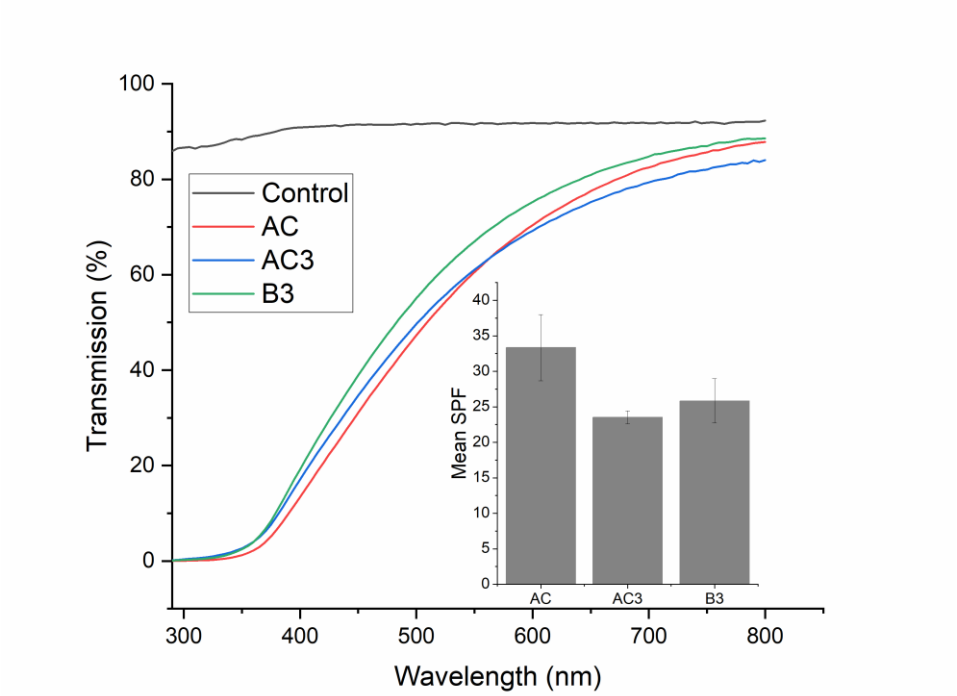

Figure 3.2.2 UV-vis transmission of pure PVA (control) and samples AC, AC3, and B3 films with LNP loading of 2.5 wt% and SPF values of AC, AC3, and B3 inset.

UV-vis properties were measured to evaluate the improved UV absorption of the acetylated sample incorporated into the films. Figure 3.2.1 shows the UV-vis transmission data for pure PVA (control), sample AC, AC3, and B3 films at 2.5 wt% loading, as well as calculated SPF values for each sample. Figure 3.2.1 shows that sample AC had the lowest transmission in the UV range (290 – 400 nm) while maintaining comparable transmission to sample B3 in the

visible range. Additionally, with an SPF of 33 for sample AC compared to 26 for sample B3, the acetylation significantly improved UV absorption performance with a t-test p-value of 0.029. During the acetylation reaction OH groups were replaced by acetyl groups, leading to a higher degree of conjugation as well as more free electrons from the additional oxygens in the acetyl groups [23], [48], [49]. The free electrons on the acetyl group undergo a lower energy n to π^*

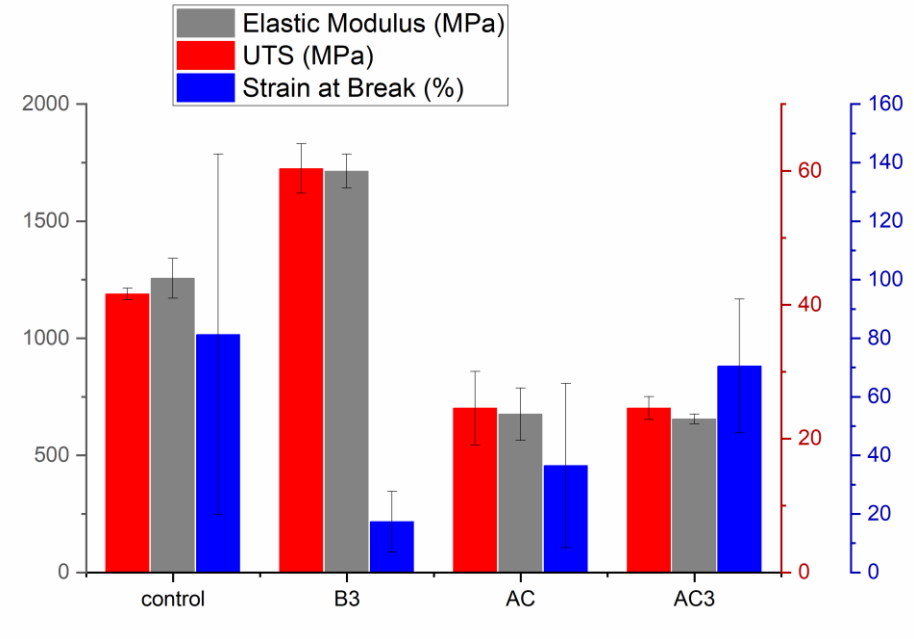

Figure 3.2.3 Tensile properties of acetylated samples (AC and AC3) compared to the pure PVA (control) and sample B3 (best performance from previous chapter).

transition leading to absorption in higher wavelengths arounds 300 nm [50], [51]. This lower energy adsorption along with an increased degree in conjugation may explain the increased UV adsorption in the 300 to 400 nm range. It is also notable that while transmission in the visible range for sample AC was comparable to that of sample B3, this slight reduction was mostly caused by an increase in particle size. With increasing particle size, particle distribution in the matrix suffered leading to less uniform light refraction, impeding transmission through the film [51]. This can be confirmed by further reduction in visible transmission for sample AC3 whose

DLS measurements showed very large particle aggregates in the range of several microns. Unlike the results seen in chapter 2, sonication of the acetylated samples led to worse UV absorption performance, likely due to sever particle aggregate formation.

Although UV performance was the main concern of this study, mechanical properties were an important factor and can influence the final products applications. Figure 3.2.2 shows the tensile data for pure PVA (control) and PVA nanocomposites loaded with 2.5 wt% of sample B3, AC, and AC3. Although samples AC and AC3 retain their plasticity (retaining comparable strain at break values), their tensile properties significantly diminish compared to the control. This is due to incorporation of hydrophobic acetyl groups into the lignin structure, leading to poor compatibility of acetylated lignin with the PVA matrix[23].

Conclusion

Using ultrasonic irradiation, it is possible to create a monodisperse lignin nanoparticle solution from alkali lignin powders. Cavitation leads to free radical reactions and those reaction pathways can be controlled via pH for different desired applications. These nanoparticles have great UV absorption properties making them a viable alternative to metal oxides as an environmentally friendly and renewable UV absorber. Additionally, their ability to mechanically reinforce a PVA composite at very low loadings makes LNPs a great option for many waterborne nanocomposites intended for UV absorbing applications. By additional functionalization it is possible to further enhance these nanoparticles via acetylation. This reaction, although not compatible for hydrophilic polymers, can greatly improve the UV adsorbing properties of lignin nanoparticles. This work has shown that through further studies and innovation, it may be possible to change lignin from a difficult biproduct to a lucrative and sought-after product.

Future Work

Future work for this study should investigate the lignin acetylation with the alkali lignin used in this study. The UV results shown in chapter 3 are very promising however mechanical reinforcement became a great hinderance in the materials applicability. To overcome this, incorporation into hydrophobic composites should be investigated. Additionally, a technoeconomic analysis and Life Cycle Assessment (LCA) of the process is highly recommended. Lignin valorization is a common goal amongst many other studies [22], [52], [53] and a Technoeconomic study would assess the feasibility of commercialization and scaling of the processes and products. The LCA will also assess the environmental impact and help determine whether the pursuit of an industry producing these products would be ethical.

References

[1] Y. Qian, X. Qiu, and S. Zhu, “Lignin: a nature-inspired sun blocker for broad-spectrum sunscreens,” *Green Chem.*, vol. 17, no. 1, pp. 320–324, Dec. 2014, doi: 10.1039/C4GC01333F.

[2] C. Kielbassa, L. Roza, and B. Epe, “Wavelength dependence of oxidative DNA damage induced by UV and visible light.,” *Carcinogenesis*, vol. 18, no. 4, pp. 811–816, Apr. 1997, doi: 10.1093/carcin/18.4.811.

[3] M. Zayat, P. Garcia-Parejo, and D. Levy, “Preventing UV-light damage of light sensitive materials using a highly protective UV-absorbing coating,” *Chem. Soc. Rev.*, vol. 36, no. 8, pp. 1270–1281, Jul. 2007, doi: 10.1039/B608888K.

[4] Y. Tu *et al.*, “Transparent and flexible thin films of ZnO-polystyrene nanocomposite for UV-shielding applications,” *J. Mater. Chem.*, vol. 20, no. 8, pp. 1594–1599, Feb. 2010, doi: 10.1039/B914156A.

[5] V. Goudarzi, I. Shahabi-Ghahfarrokhi, and A. Babaei-Ghazvini, “Preparation of ecofriendly UV-protective food packaging material by starch/TiO2 bio-nanocomposite: Characterization,” *Int. J. Biol. Macromol.*, vol. 95, pp. 306–313, Feb. 2017, doi: 10.1016/j.ijbiomac.2016.11.065.

[6] B. C. Heng, X. Zhao, S. Xiong, K. Woei Ng, F. Yin-Chiang Boey, and J. Say-Chye Loo, “Toxicity of zinc oxide (ZnO) nanoparticles on human bronchial epithelial cells (BEAS-2B) is accentuated by oxidative stress,” *Food Chem. Toxicol.*, vol. 48, no. 6, pp. 1762–1766, Jun. 2010, doi: 10.1016/j.fct.2010.04.023.

[7] Y. Xiao, M. G. Vijver, G. Chen, and W. J. G. M. Peijnenburg, “Toxicity and Accumulation of Cu and ZnO Nanoparticles in Daphnia magna,” *Environ. Sci. Technol.*, vol. 49, no. 7, pp. 4657–4664, Apr. 2015, doi: 10.1021/acs.est.5b00538.

[8] J. C. Yu, Yu, Ho, Jiang, and Zhang, “Effects of F- Doping on the Photocatalytic Activity and Microstructures of Nanocrystalline TiO2 Powders,” *Chem. Mater.*, vol. 14, no. 9, pp. 3808–3816, Sep. 2002, doi: 10.1021/cm020027c.

[9] Y. Wang *et al.*, “Simultaneous Enhancements of UV-Shielding Properties and Photostability of Poly(vinyl alcohol) via Incorporation of Sepia Eumelanin,” *ACS Sustain. Chem. Eng.*, vol. 4, no. 4, pp. 2252–2258, Apr. 2016, doi: 10.1021/acssuschemeng.5b01734.

[10] M. Tortora, F. Cavalieri, P. Mosesso, F. Ciaffardini, F. Melone, and C. Crestini, “Ultrasound Driven Assembly of Lignin into Microcapsules for Storage and Delivery of Hydrophobic Molecules,” *Biomacromolecules*, vol. 15, no. 5, pp. 1634–1643, May 2014, doi: 10.1021/bm500015j.

[11] H. Sadeghifar and A. Ragauskas, “Lignin as a UV Light Blocker—A Review,” *Polymers*, vol. 12, no. 5, Art. no. 5, May 2020, doi: 10.3390/polym12051134.

[12] K. Shikinaka, M. Nakamura, and Y. Otsuka, “Strong UV absorption by nanoparticulated lignin in polymer films with reinforcement of mechanical properties,” *Polymer*, vol. 190, p. 122254, Mar. 2020, doi: 10.1016/j.polymer.2020.122254.

[13] F. Xiong, Y. Wu, G. Li, Y. Han, and F. Chu, “Transparent Nanocomposite Films of Lignin Nanospheres and Poly(vinyl alcohol) for UV-Absorbing,” *Ind. Eng. Chem. Res.*, vol. 57, no. 4, pp. 1207–1212, Jan. 2018, doi: 10.1021/acs.iecr.7b04108.

[14] B. Wang, D. Sun, H.-M. Wang, T.-Q. Yuan, and R.-C. Sun, “Green and Facile Preparation of Regular Lignin Nanoparticles with High Yield and Their Natural Broad-

Spectrum Sunscreens," *ACS Sustain. Chem. Eng.*, vol. 7, no. 2, pp. 2658–2666, Jan. 2019, doi: 10.1021/acssuschemeng.8b05735.
[15] W. Yang *et al.*, "Antioxidant and antibacterial lignin nanoparticles in polyvinyl alcohol/chitosan films for active packaging," *Ind. Crops Prod.*, vol. 94, pp. 800–811, Dec. 2016, doi: 10.1016/j.indcrop.2016.09.061.
[16] W. Yang *et al.*, "Polyvinyl alcohol/chitosan hydrogels with enhanced antioxidant and antibacterial properties induced by lignin nanoparticles," *Carbohydr. Polym.*, vol. 181, pp. 275–284, Feb. 2018, doi: 10.1016/j.carbpol.2017.10.084.
[17] X. He *et al.*, "Thermal, antioxidant and swelling behaviour of transparent polyvinyl (alcohol) films in presence of hydrophobic citric acid-modified lignin nanoparticles," *Int. J. Biol. Macromol.*, vol. 127, pp. 665–676, Apr. 2019, doi: 10.1016/j.ijbiomac.2019.01.202.
[18] X. Zhang, W. Liu, W. Liu, and X. Qiu, "High performance PVA/lignin nanocomposite films with excellent water vapor barrier and UV-shielding properties," *Int. J. Biol. Macromol.*, vol. 142, pp. 551–558, Jan. 2020, doi: 10.1016/j.ijbiomac.2019.09.129.
[19] S. Kubo and J. F. Kadla, "The Formation of Strong Intermolecular Interactions in Immiscible Blends of Poly(vinyl alcohol) (PVA) and Lignin," *Biomacromolecules*, vol. 4, no. 3, pp. 561–567, May 2003, doi: 10.1021/bm025727p.
[20] J. H. Finley, "Spectrophotometric determination of polyvinyl alcohol in paper coatings," *Anal. Chem.*, vol. 33, no. 13, pp. 1925–1927, Dec. 1961, doi: 10.1021/ac50154a044.
[21] M. N. G. Gonzalez, M. Levi, S. Turri, and G. Griffini, "Lignin nanoparticles by ultrasonication and their incorporation in waterborne polymer nanocomposites," *J. Appl. Polym. Sci.*, vol. 134, no. 38, p. 45318, 2017, doi: https://doi.org/10.1002/app.45318.
[22] D. Tian, J. Hu, J. Bao, R. P. Chandra, J. N. Saddler, and C. Lu, "Lignin valorization: lignin nanoparticles as high-value bio-additive for multifunctional nanocomposites," *Biotechnol. Biofuels*, vol. 10, no. 1, p. 192, Jul. 2017, doi: 10.1186/s13068-017-0876-z.
[23] Y. Kim *et al.*, "All Biomass and UV Protective Composite Composed of Compatibilized Lignin and Poly (Lactic-acid)," *Sci. Rep.*, vol. 7, no. 1, Art. no. 1, Mar. 2017, doi: 10.1038/srep43596.
[24] I. A. Gilca, V. I. Popa, and C. Crestini, "Obtaining lignin nanoparticles by sonication," *Ultrason. Sonochem.*, vol. 23, pp. 369–375, Mar. 2015, doi: 10.1016/j.ultsonch.2014.08.021.
[25] "Cavitation mechanism of ultrasonic melt degassing," *Ultrason. Sonochem.*, vol. 2, no. 2, pp. S137–S141, Jan. 1995, doi: 10.1016/1350-4177(95)00020-7.
[26] A. Casas, M. V. Alonso, M. Oliet, E. Rojo, and F. Rodríguez, "FTIR analysis of lignin regenerated from Pinus radiata and Eucalyptus globulus woods dissolved in imidazolium-based ionic liquids," *J. Chem. Technol. Biotechnol.*, vol. 87, no. 4, pp. 472–480, 2012, doi: https://doi.org/10.1002/jctb.2724.
[27] M. Mousa and Y. Dong, "Strong Poly(Vinyl Alcohol) (PVA)/Bamboo Charcoal (BC) Nanocomposite Films with Particle Size Effect," *ACS Sustain. Chem. Eng.*, vol. 6, no. 1, pp. 467–479, Jan. 2018, doi: 10.1021/acssuschemeng.7b02750.
[28] M. Lievonen *et al.*, "A simple process for lignin nanoparticle preparation," *Green Chem.*, vol. 18, no. 5, pp. 1416–1422, Feb. 2016, doi: 10.1039/C5GC01436K.
[29] O. Derkacheva and D. Sukhov, "Investigation of Lignins by FTIR Spectroscopy," *Macromol. Symp.*, vol. 265, no. 1, pp. 61–68, 2008, doi: https://doi.org/10.1002/masy.200850507.

[30] B. D. Mar and H. J. Kulik, “Depolymerization Pathways for Branching Lignin Spirodienone Units Revealed with ab Initio Steered Molecular Dynamics,” *J. Phys. Chem. A*, vol. 121, no. 2, pp. 532–543, Jan. 2017, doi: 10.1021/acs.jpca.6b11414.
[31] J. Coates, “Interpretation of Infrared Spectra, A Practical Approach,” *Encycl. Anal. Chem.*, Sep. 2006.
[32] “The effect of pH on the conversion of superoxide to hydroxyl free radicals,” *Arch. Biochem. Biophys.*, vol. 234, no. 1, pp. 258–264, Oct. 1984, doi: 10.1016/0003-9861(84)90348-5.
[33] L. Mbanga, M. Mulenga, P. T. Mpiana, K. Bokolo, M. Mumbwa, and K. Mvingu, “Determination of Sun Protection Factor (SPF) of Some Body Creams and Lotions Marketed in Kinshasa by Ultraviolet Spectrophotometry,” *Int. J. Adv. Res. Chem. Sci.*, vol. 1, no. 8, pp. 2349–0403, Oct. 2014.
[34] R. Zhong and K. Wille, “Equal Arc Segment Method for Averaging Data Plots Exemplified for Averaging Stress versus Strain Curves of Pervious Concrete,” *J. Mater. Civ. Eng.*, vol. 28, no. 1, p. 04015071, Jan. 2016, doi: 10.1061/(ASCE)MT.1943-5533.0001345.
[35] L. Jiang, Y. Liao, Q. Wan, and W. Li, “Effects of sintering temperature and particle size on the translucency of zirconium dioxide dental ceramic,” *J. Mater. Sci. Mater. Med.*, vol. 22, no. 11, pp. 2429–2435, Nov. 2011, doi: 10.1007/s10856-011-4438-9.
[36] T. Soderberg, “The Effect of Conjugation on λmax,” in *Organic Chemistry with a Biological Emphasis*, vol. I, Chemistry Publications, 2019.
[37] P. Posoknistakul *et al.*, “Fabrication and Characterization of Lignin Particles and Their Ultraviolet Protection Ability in PVA Composite Film,” *ACS Omega*, vol. 5, no. 33, pp. 20976–20982, Aug. 2020, doi: 10.1021/acsomega.0c02443.
[38] Y. Zhang, R. Remadevi, J. P. Hinestroza, X. Wang, and M. Naebe, “Transparent Ultraviolet (UV)-Shielding Films Made from Waste Hemp Hurd and Polyvinyl Alcohol (PVA),” *Polymers*, vol. 12, no. 5, Art. no. 5, May 2020, doi: 10.3390/polym12051190.
[39] K. Petersen *et al.*, “Potential of biobased materials for food packaging,” *Trends Food Sci. Technol.*, vol. 10, no. 2, pp. 52–68, Feb. 1999, doi: 10.1016/S0924-2244(99)00019-9.
[40] C. Lu, C. Blackwell, Q. Ren, and E. Ford, “Effect of the Coagulation Bath on the Structure and Mechanical Properties of Gel-Spun Lignin/Poly(vinyl alcohol) Fibers,” *ACS Sustain. Chem. Eng.*, vol. 5, no. 4, pp. 2949–2959, Apr. 2017, doi: 10.1021/acssuschemeng.6b02423.
[41] M. R. Kaizer, A. de Oliveira-Ogliari, M. S. Cenci, N. J. M. Opdam, and R. R. Moraes, “Do nanofill or submicron composites show improved smoothness and gloss? A systematic review of in vitro studies,” *Dent. Mater.*, vol. 30, no. 4, pp. e41–e78, Apr. 2014, doi: 10.1016/j.dental.2014.01.001.
[42] K. Kanimozhi, S. Khaleel Basha, and V. Sugantha Kumari, “Processing and characterization of chitosan/PVA and methylcellulose porous scaffolds for tissue engineering,” *Mater. Sci. Eng. C*, vol. 61, pp. 484–491, Apr. 2016, doi: 10.1016/j.msec.2015.12.084.
[43] J. M. Yang, W. Y. Su, T. L. Leu, and M. C. Yang, “Evaluation of chitosan/PVA blended hydrogel membranes,” *J. Membr. Sci.*, vol. 236, no. 1, pp. 39–51, Jun. 2004, doi: 10.1016/j.memsci.2004.02.005.
[44] S. S. Nair *et al.*, “High Shear Homogenization of Lignin to Nanolignin and Thermal Stability of Nanolignin-Polyvinyl Alcohol Blends,” *ChemSusChem*, vol. 7, no. 12, pp. 3513–3520, Dec. 2014, doi: 10.1002/cssc.201402314.

[45] N. Zhang, P. Tao, Y. Lu, and S. Nie, “Effect of lignin on the thermal stability of cellulose nanofibrils produced from bagasse pulp,” *Cellulose*, vol. 26, no. 13, pp. 7823–7835, Sep. 2019, doi: 10.1007/s10570-019-02657-w.
[46] A. K. Patel, R. Bajpai, and J. M. Keller, “On the crystallinity of PVA/palm leaf biocomposite using DSC and XRD techniques,” *Microsyst. Technol.*, vol. 20, no. 1, pp. 41–49, Jan. 2014, doi: 10.1007/s00542-013-1882-0.
[47] M. Borhani zarandi, H. Amrollahi Bioki, Z. Mirbagheri, F. Tabbakh, and G. Mirjalili, “Effect of crystallinity and irradiation on thermal properties and specific heat capacity of LDPE & LDPE/EVA,” *Appl. Radiat. Isot.*, vol. 70, no. 1, pp. 1–5, Jan. 2012, doi: 10.1016/j.apradiso.2011.09.001.
[48] S. Pietrzyk, L. Juszczak, T. Fortuna, and A. Ciemniewska, “Effect of the oxidation level of corn starch on its acetylation and physicochemical and rheological properties,” *J. Food Eng.*, vol. 120, pp. 50–56, Jan. 2014, doi: 10.1016/j.jfoodeng.2013.07.013.
[49] S. K. Karatzos, L. A. Edye, and R. M. Wellard, “The undesirable acetylation of cellulose by the acetate ion of 1-ethyl-3-methylimidazolium acetate,” *Cellulose*, vol. 19, no. 1, pp. 307–312, Feb. 2012, doi: 10.1007/s10570-011-9621-0.
[50] F. A. Carey, *Organic chemistry*, Ninth edition. New York, NY: McGraw-Hill, 2014.
[51] L. Zhao *et al.*, “Solution-Processed VO 2 -SiO 2 Composite Films with Simultaneously Enhanced Luminous Transmittance, Solar Modulation Ability and Anti-Oxidation property,” *Sci. Rep.*, vol. 4, no. 1, Art. no. 1, Nov. 2014, doi: 10.1038/srep07000.
[52] J. G. Linger *et al.*, “Lignin valorization through integrated biological funneling and chemical catalysis,” *Proc. Natl. Acad. Sci. U. S. A.*, vol. 111, no. 33, pp. 12013–12018, 2014.
[53] A. J. Ragauskas *et al.*, “Lignin Valorization: Improving Lignin Processing in the Biorefinery,” *Science*, vol. 344, no. 6185, May 2014, doi: 10.1126/science.1246843.